Research Square

Preprints are preliminary reports that have not undergone peer review.
They should not be considered conclusive, used to inform clinical practice,
or referenced by the media as validated information.

Timing and cause of early Late Pleistocene megadrought in eastern Africa

Verschuren D

dirk.verschuren@UGent.be

Ghent University https://orcid.org/0000-0002-9116-5446

Baxter AJ

Utrecht University

Peterse F

Utrecht University

Yin QZ

Université Catholique de Louvain

Van Daele M

Ghent University

Van der Meeren T

Ghent University

Wu ZP

Université Catholique de Louvain

Olago DO

University of Nairobi

Barker PA

Lancaster University

Damste JSS

NIOZ Royal Netherlands Institute for Sea Research

Research Article

Keywords: Late Pleistocene, MIS5 megadrought, African paleoclimate, Horn of Africa, Lake Chala

Posted Date: July 3rd, 2026

DOI: https://doi.org/10.21203/rs.3.rs-10224410/v1

License: This work is licensed under a Creative Commons Attribution 4.0 International License.
Read Full License

Additional Declarations: The authors declare no competing interests.

Abstract

During the early Late Pleistocene period between ~ 135,000 and ~ 70,000 years ago (~ 135 – 70 kyr ago) tropical Africa experienced several episodes of prolonged drought that must have impacted the living environment of ancient modern humans and may have triggered their dispersal towards, and into, Eurasia. The causal mechanism of these megadroughts remains elusive, in part because prevailing (near-) interglacial temperatures are expected to have intensified tropical monsoons, rather than instigate drought. Here we use sedimentary organic-geochemical data from Lake Chala near Mt. Kilimanjaro to reconstruct climate evolution over the last 170 kyr in eastern equatorial Africa, a region lacking direct oceanic teleconnection to northern high-latitude climate feedbacks. We find that temperature variation was strongly influenced by atmospheric greenhouse-gas concentrations and global glaciation extent, especially in the last ~ 80 kyr when low orbital eccentricity muted the influence of precession on local insolation. Last Interglacial temperature peaked ~ 130 kyr ago and also ~ 110 kyr ago, even though by that time incipient glaciation and increasing atmospheric dust already generated positive feedbacks on the global cooling caused by a ~ 50 ppm decline in atmospheric CO_2. We suggest that the coincidence of high atmospheric moisture deficit over eastern equatorial Africa with cool sea-surface temperature in the Arabian Sea moisture source area of the northeasterly monsoon curtailed the short rain season and led to a single period of extreme drought between 110 ± 2.0 and 97 ± 1.6 kyr ago.

Introduction

Natural climate archives from throughout tropical Africa contain evidence that the early Late Pleistocene period ~135-70 kyr ago (broadly Marine Isotope Stage [MIS] 5) was punctuated by several multi-millennial episodes of severe climatic drought (*1-2*), which must have impacted the living environment and, hence, dispersal of ancient modern humans (*3*). Potentially, these so-called MIS5 African megadroughts (*4*) may even have triggered early human migration to northeastern Africa and into Eurasia (*2*; Supplementary text). The causal mechanism of these extreme droughts has remained a mystery, not least because the surface temperature of tropical oceans and continents at that time was comfortably high enough for invigorated monsoon dynamics (*5*) to have generated adequate precipitation and thus relatively moist continental climate regimes. Yet climate-proxy records from long-lived lakes in eastern Africa (*1,6-7*) indicate that MIS5 megadroughts were substantially more severe than the relative aridity that occurred during the Last Glacial Maximum (LGM, 23-19 kyr ago) when pronounced temperature depression (~3-4 °C at sea level compared to today; *8*) curtailed the production and delivery of monsoonal moisture (*9*). Elucidating the causal mechanism of the MIS5 African megadroughts has been hampered by the difficulty of dating lake-sediment records from this period with sufficient precision, compounded by discontinuity of climate-proxy registration at many sites, partly a consequence of the drought episodes' severe aridity. As a result, it has proved challenging to assess the regional and continental synchrony of megadrought events recorded at individual sites (*3*), or to relate these sites' climate-proxy records to variation in local and extratropical orbital insolation forcing (*10*).

Here we present paired temperature and hydroclimate reconstructions for eastern equatorial Africa spanning the last 170 kyr with on average 200-year resolution, based on variation in the distributions of branched glycerol dialkyl glycerol tetraethers (brGDGTs) in the continuous (*11*) sediment record of Lake Chala (3.3° S, 37.7° E). Located east of the Congo Air Boundary (CAB) year-round (Fig. 1), past climate dynamics registered at this location can be considered aligned with the Horn of Africa region of eastern Africa that is fully dependent on Indian Ocean moisture (*12*). Annual rainfall has a bimodal distribution with two rainy seasons (March–May and October–December) and a distinct dry season during boreal summer (June–September) (Fig. S1). GDGTs are membrane lipids produced by bacteria and archaea that preserve well in lake and marine sediments and are widely applied in palaeoclimate research (*13*). We reconstructed mean summer temperature (MST) using a calibration based on the distribution of branched GDGTs (brGDGTs) in a set of globally distributed lakes (*14*) that we previously established to best capture past temperature variation in this setting (*15-16*; Methods). Reconstruction of past hydroclimate changes is based on the branched and isoprenoid tetraether (BIT) index which expresses the abundance ratio between brGDGTs and a specific isoprenoid GDGT, crenarchaeol (*17*; Methods). In the setting of Lake Chala and at the time scale considered here, the BIT index is a proxy for climatic moisture balance (precipitation minus evaporation, P–E), because a surplus of P over E enhances the overland flow and groundwater recharge, which eventually leads to greater lake depth and stronger water-column stratification, in turn affecting the relative niche availability for brGDGT-producing bacteria and crenarchaeol-producing Nitrosphaerota (*18*) that drive this index (*15,19-20*). Our climate-proxy time series are supported by a fully independent (i.e., untuned to external chronologies) age model integrating the results of high-resolution radiocarbon (^{14}C) dating (*21*), argon ($^{40}Ar/^{39}Ar$) dating of 10 primary ashfall horizons (*22*) and sedimentary signatures of six geomagnetic intensity excursions (*23*) with the precise time anchor provided by local cryptotephra of the Toba volcanic eruption in Indonesia 73.7 kyr ago (*15*) (Methods). The resulting chronology (Fig. S2) is sufficiently well-constrained (2-sigma age uncertainty $\pm$1625 years on average, maximally $\pm$3100 years) to compare our temperature and hydroclimate reconstructions directly with variation in orbital insolation parameters (*24*), and with time series of atmospheric CO_2 and high-latitude temperature variation registered in polar ice caps (*25*-27), the deep-ocean record of global glaciation extent (*28*), and selected climate-proxy records from tropical and mid-latitude regions. Insights from these comparisons supplemented by HadCM3 simulations of geographical and seasonal climate anomalies (*29*) allow us to identify a causal mechanism for the most severe MIS5 megadrought episode in eastern Africa.

The last glacial-interglacial cycle in eastern equatorial Africa

As registered in Lake Chala, the temperature history of eastern equatorial Africa over the past 170 kyr (Fig. 2f) displays the principal features of a late Quaternary glacial-interglacial cycle, with relatively modest multi-millennial fluctuations bracketed by two large-amplitude temperature increases marking the ends of the most recent and penultimate ice ages. Using the signatures of these ice-age

terminations (T1 and T2) in the marine oxygen-isotope ($d^{18}O$) record of global ice volume (*28*) as benchmarks, postglacial warming in eastern equatorial Africa associated with T1 started at 14.0±0.4 kyr ago, following strong regional cooling during Heinrich Stadial 1 (HS1, 18-15 kyr ago). The onset of warming associated with T2 is dated to 142.2±2.9 kyr ago. Given dating uncertainty, this is coeval with the onset of rapid warming in Antarctica (*27,30*), and thus ~10 kyr earlier than the onset of rapid warming in Greenland (*26*). MST values representing peak glacial cooling during MIS6 (21.5±0.7 °C) are slightly less depressed than those towards the end of MIS2 (LGM: 20.4±0.7 °C) and during a cool episode ~57-49 kyr ago (20.7±0.7 °C). Other cool episodes (MST often <22.5 °C) are dated to ~120-118, ~85-80 and ~34-31 kyr ago (Fig. 2f). Peak interglacial MSTs (consistently >24 °C) are reached ~135-128 kyr ago and during the mid-Holocene, 8-4 kyr ago (Fig. 2f), with peak warmth at 130.8±2.7 kyr ago being coeval, within dating uncertainty, with last-interglacial temperature maxima in both Antarctica and Greenland (Fig. 2b, 2h). Maximum last-interglacial MST values (25.7±0.7 °C) are barely higher than peak Holocene warmth (25.1±0.7 °C), consistent with regionally resolved global inventories indicating that sub-stage MIS5e (the Last Interglacial [LIG] period as commonly defined) was globally warmer than the pre-industrial current interglacial mostly because of polar amplification (*31-32*). Notably, a temperature regime that, using the Holocene as reference, can be considered fully interglacial (MST consistently >23 °C) also occurred between ~112 and ~100 kyr ago, during the phase of incipient glaciation following the LIG. Apart from the above-mentioned cool phases, MST in equatorial eastern Africa hovered between 22.5 and 23 °C from ~100 kyr ago until the end of the last glacial period. With regard to its general structure, our 170-kyr MST time series from Lake Chala is intermediate between the temperature records of Antarctica (Fig. 2h) and Greenland (Fig. 2b). Temperatures in this equatorial region being less depressed during MIS6 than during MIS2 is more in line with the southern high-latitude record (*27*), suggesting that the near-equal minimum and maximum $\delta^{18}O$ values bracketing T2 and T1 in the benthic marine $d^{18}O$ stack (*28*; Fig. 2a) may obscure a distinct difference in maximum continental ice volume between the penultimate glaciation and the last glaciation.

Focusing on the timing of temperature fluctuations (Fig. 2f) in relation to insolation forcing at the Equator, five successive MST maxima and minima between ~160 and ~110 kyr ago are broadly in-phase with insolation variation at the March equinox, whereas the three most recent MST fluctuations (two maxima and one minimum in the last ~30 kyr) are in-phase with insolation variation at the September equinox (Fig. 2e). During the intervening period (~110-30 kyr ago), changes in MST do not appear to trace either March or September insolation, except for the cool episode ~57-49 kyr ago (Fig. 2f), which matches a minimum in March insolation. Over the entire 170 kyr record, MST variability displays some periodicity indicative of precessional (~21-kyr) forcing, but less pronounced than periodicity in frequency bands with no obvious link to orbital insolation parameters (Fig. S3). Precession-band periodicity is largely due to MST highs (and lows) being spaced at ~23-kyr intervals (Fig. 2f), masking the apparent incongruence that the earlier MST excursions are in-phase with local March insolation, while the more recent ones are in-phase with local September insolation. At first glance, this phase shift might suggest that while orbital-scale temperature variation in eastern equatorial Africa is now most sensitive to peak seasonal insolation moving south at the end of boreal summer (*33*), during MIS5 it was most sensitive to

peak seasonal insolation moving north at the end of austral summer. This would partly explain why T2 warming at the Equator occurred early, coeval with warming in Antarctica, while the timing of T1 warming is more similar to that in Greenland (Fig. 2f). Sensitivity of equatorial temperature variation to local insolation also explains the relative brevity of peak LIG warmth (~4 kyr) compared with high-latitude regions where it lasted ~12-15 kyr (Fig. 2b, 2h). This mirrors the Holocene situation when peak MST values were concentrated in the period between 8 and 4 kyr ago (*15*). Fading of the precessional signal in equatorial temperature after ~100 kyr ago conforms to expectation, as diminishing eccentricity of Earth's orbit restricted the amplitude of insolation variability due to precession (*1*). However, as low eccentricity prevailed until the present (Fig. 2e), this scenario fails to explain why a precessional signal reappeared in the last ~30 kyr, and why it shifted phase compared to MIS5. We propose instead that the recent 'phase lock' with local September insolation may be an artifact of HS1-associated regional cooling 18-14 kyr ago occurring halfway between elevated pre-LGM temperatures ~31-27 ka BP and peak mid-Holocene warming (Fig. 2e-f).

Excluding the above-mentioned cold spells, our data suggest that equatorial eastern Africa enjoyed a rather mild glacial temperature regime (MST on average 1.2 °C lower than during the Holocene) from ~100 kyr ago (Fig. 2f), with no further cooling around 70 kyr ago (i.e., at the start of MIS4). This contrasts with extratropical regions of both hemispheres, where by that time strongly expanded northern-hemisphere ice caps (as reflected in the benthic-marine $d^{18}O$ record; Fig. 2a) and elevated atmospheric dust levels (*34*; Fig. 2j) created positive feedback on decreasing greenhouse-gas forcing (Fig. 2i) to generate additional cooling during MIS4-MIS2 (Fig. 2b, 2h).

Shifts through time in the relationship between moisture balance and temperature

The Chala BIT-index record (Fig. 3d) indicates that both glacial and interglacial phases in eastern equatorial Africa were characterised by major variation in moisture balance. In the Holocene, driest conditions coincided with peak mid-Holocene warmth 8-4 kyr ago (*15*). During the last glacial period between ~75 and 11.7 kyr ago, climate conditions were often wetter than today but interrupted by dry episodes (BIT-index values consistently <0.4) ~53-50 kyr ago, 20.5-16 kyr ago (partly offset from the LGM but overlapping with HS1; *35*) and during the Younger Dryas (YD, 12.9-11.7 kyr ago) (Fig. 3d). In the Lake Chala record prior to ~75 kyr ago, BIT-index values are bimodally distributed, with long sections of low values (<0.4) alternating with sections of strongly fluctuating values that occasionally exceed 0.8 (Fig. 3d) (Supplementary text). Within the MIS5 time window, BIT-index values are consistently low (<0.4) during three intervals dated to ~136-123 kyr ago, ~110-87 kyr ago and ~85-77 kyr ago (Fig. 3d). The second of these intervals coincides with a prolonged low-stand of Lake Chala registered in seismic stratigraphy (*7,11*), dated to between 110$\pm$2.0 and 88$\pm$1.7 kyr ago (Fig. S2 and vertical shading in Fig. 3). BIT-index values are particularly low (mean 0.15, range 0.06-0.21) during the main phase of this low-stand ~110-97.5 kyr ago, meaning that the water column of Lake Chala at that time was too shallow to provide the truly anoxic niche required by local brGDGT-producing bacteria (*16,19*).

A notable feature of our paired temperature-hydroclimate reconstruction is that a generally positive relationship between effective moisture (represented by the BIT index) and temperature (represented by MST) during the last glacial period (75-11.7 kyr ago) shifted to negative in the Holocene (*15*). Using a sliding correlation window of 3-10 kyr (*36*) to trace this relationship in greater temporal detail, we find that variation in moisture and temperature show a consistently positive relationship only in the latter half of the glacial period (~35 to 11.7 kyr ago), and alternated between positive and negative in the early part (~75 to ~35 kyr ago) (Fig. 3g). Importantly, in the portion of the record dated to before ~90 kyr ago, the relationship is predominantly negative, as in the Holocene. This suggests that eastern equatorial Africa experienced a climate regime broadly similar to that of the current interglacial (and today: Fig. 1) throughout MIS5. Indeed, MST values between ~112 and ~101 kyr ago were on average 23.7 °C, near-identical to both the reconstructed Holocene average (23.6 °C) and present-day mean annual temperature near Lake Chala (23.7 °C; *37*).

A causal mechanism for MIS5 African megadrought

Warmest Last Interglacial conditions in eastern equatorial Africa ~135-128 kyr ago coincided with local March insolation peaking 132 kyr ago. The warm phase dated to ~112-101 kyr ago is not centred over the next March insolation peak 111 kyr ago but ~4000 years later, rendering it broadly coeval with a similarly long-lasting (~10-kyr) positive SST excursion off western equatorial Africa (Fig. 2d) and with an episode of strong East Asian monsoon activity (Fig. 3a) triggered by high boreal summer insolation (Figs. 2c, 3b) (*38*). Given that by ~110 kyr ago (halfway through MIS5d) incipient glaciation ending the Last Interglacial period (MIS5e) had already significantly cooled both northern and southern high-latitude regions (about half of the total glacial-interglacial ΔT: compare Figs. 2b and 2h with Fig. 2i), the meridional temperature gradient at that time must have been exceptionally steep. HadCM3 climate simulations (*29*) indicate that 105 kyr ago the difference in mean-annual SST between the western equatorial Indian Ocean and the Arabian Sea, in particular, may have been ~2 °C greater than today (Fig. 4a) (Supplementary Information). Combining this climate-model output with our temporally constrained climate reconstruction (Figs. 2-3), we propose that the coincidence of already declining SSTs in the Arabian Sea source region of monsoon moisture with still elevated (i.e., interglacial-style) atmospheric moisture demand over eastern equatorial Africa may have undercut on-land precipitation, thereby creating a period of extremely low effective moisture registered as the principal MIS5 African megadrought. At Lake Chala it is expressed as the ~12,000-year period between 110$\pm$2.0 and 97.5$\pm$0.5 kyr ago when lake depth was most strongly reduced (Fig. S2 and orange vertical shading in Fig. 3), and BIT-index values are consistently <0.20 (Fig. 3d). In seismic stratigraphy the low-stand is seen to persist after ~98 kyr ago in a condition of less extreme lake-level lowering (except for a brief interval ~96-94 kyr ago; Fig. 3), indicating at least modest improvement of the lake's water balance and hence, less negative climatic moisture balance. In agreement with this data, BIT-index values remain low (<0.40) until ~87 kyr ago but less extremely so compared with the period ~110-97.5 kyr ago.

The proposed mechanism for development of megadrought conditions may appear counter-intuitive, considering that the enhanced temperature contrast between equatorial eastern Africa and at least one

of its oceanic moisture sources might be expected to have generated more, not less, precipitation. However, as equatorial MST values ~112-101 kyr ago were comparable to those attained during the Holocene (Fig. 2f) and today (Fig. 1), a similar climate regime prevailed with predominantly negative relationship between effective moisture and temperature (Fig. 3f). Thus it appears that, like today (Fig.1), water availability did not suffice for terrestrial evaporation to meet the high moisture demand of the warm atmosphere (*39*), in turn inhibiting precipitation of newly advected moisture (*40*). Moreover, compared to other monsoon systems the eastern African monsoons are rather dry, because northeasterly monsoon winds originate above relatively cool surface waters of the Arabian Sea, while southeasterly monsoon winds already lose much of their humidity near the East African coast before entering the continent (*41*; Fig. S1). Cumulative rainfall deficits over multiple years lead to declines in groundwater recharge and overland flow that eventually result in major lake low-stands testifying to a long period of persistently negative climatic moisture balance (*15*). Judging by our data, this interglacial-style hydroclimate prevailed until ~90 kyr ago, followed by a ~10-kyr period with limited correlation between moisture and temperature (Fig. 3g). Around ~80 kyr ago, equatorial eastern Africa assumed a glacial-style hydroclimate with most often positive relationship between moisture and temperature, in line with monsoon theory (*5*) and thus apparently more limited impact of thermodynamic effects on continental precipitation. Coincidence of a century-scale drying trend at Lake Chala with northern high-latitude cooling in a ~450-year time window encompassing the Toba eruption 73.7 kyr ago (*42*) supports our data that this glacial-style hydroclimate already prevailed before the end of MIS5 (Fig. 3g).

Focusing on the seasonal timing of rainfall deficits during this MIS5 megadrought, we note that northeasterly monsoon winds advecting moisture in October-December (delivering the 'short' rains) tend to approach the eastern African landmass from a more meridional direction than the southeasterly monsoon winds advecting moisture in March-May (the 'long' rains) (*41*; Fig. S1). Therefore, the short rains were probably more susceptible to the monsoon-dampening effect of a steep latitudinal temperature gradient. In the portion of eastern tropical Africa depending entirely or predominantly on Indian Ocean moisture the mechanism for megadrought generation proposed here thus most likely involved (partial) failure of the short rains brought on-land by the northeasterly monsoon. In addition, moisture generation in the Arabian Sea was likely lowest during boreal winter, thereby curtailing the short rain season and resulting in earlier onset, and longer duration, of the short dry season in eastern Africa. HadCM3 simulation of rainfall seasonality in the Lake Chala area 105 kyr ago indeed suggests precipitation to have been depressed from December until March (Fig. 4b), although this may have been compensated partly by enhancement of the long rain season, relative to today, due to high northern hemisphere summer insolation at that time (Fig. 2c).

MIS5 African megadroughts reflected in lake low-stands

If megadrought conditions ~110-97.5 kyr ago as recorded at Lake Chala were caused primarily by failure of the northeasterly monsoon, they can be expected to have been limited to the area of eastern Africa located north of the tropical rain belt and east of the CAB at least part of the year, i.e. the greater Horn of Africa region and much of the East African plateau to ~10° S latitude (Fig. 1). Yet MIS5 megadrought

events have been documented from throughout intertropical Africa, to ~20° S and including portions of the continent fully dependent on Atlantic Ocean moisture (*3*). This would suggest that megadrought conditions do not depend solely on (partial) failure of one or both of the eastern African monsoons. Also, the number and timing of inferred MIS5 megadroughts varies among sites, implying that different climate-dynamical mechanisms may be involved. With dating uncertainty of these events often exceeding their inferred duration (Supplementary text), regional integration of the available palaeodata is not feasible at this time. Here we refer only to the sedimentary record of Lake Tanganyika (6.7° S, 29.8° E), the only other climate archive in eastern Africa with demonstrably continuous lacustrine deposition throughout the ~70-kyr time window covered by MIS5 (*6*) and therefore most compatible with our data. Like Lake Chala, Lake Tanganyika experienced a single major MIS5 low-stand (Fig. 3d), which lasted from (shortly) before ~106 kyr ago until the onset of transgression sometime after ~97±6 kyr ago; this was followed by slow lake-level rise to reach near-modern levels by ~70 kyr ago (*1,6*). The apparent absence of MIS5 megadrought evidence in eastern Africa north of the equator may be due to lack of continuous climate archives there (*3*). Sedimentary proxy data from Chew Bahir in eastern Ethiopia (4.6° N, 37.0° E) are indicative of predominantly wet climate conditions between ~143±17 and ~79±8 kyr ago (*43-44*), suggesting that hydroclimate history in at least the northern part of its drainage basin conforms to records from northeastern Africa and the Arabian Peninsula (*45*; Supplementary text).

Evaluating MIS5 megadrought signatures in climate records from outside eastern equatorial Africa is equally challenging, and beyond the scope of the present study. Moreover, although also western equatorial Africa experienced elevated temperatures in the period ~110-100 kyr ago (*46*; Fig. 2d), eastern African megadroughts did not necessarily extend to the Atlantic side of the continent, given more restricted seasonal latitudinal migration of the tropical rain belt there (Fig. 1) and different geography of tropical land mass relative to the trajectory of the African monsoon (Fig. S1). For example, a reconstruction of vegetation history around Lake Bosumtwi (1.4° N, 1.4° W) shows that fairly moist conditions prevailed there between ~130 and ~100 kyr ago (*47*), i.e. including the principal MIS5 megadrought period in eastern Africa. Sedimentary evidence of a pronounced low-stand, possibly even complete desiccation, of Lake Bosumtwi is limited to a ~4000-year interval centred on (maximally) 77.9±6.1 kyr ago (*1,48*). This suggests that the interglacial temperature regime peaking ~127-123 and ~110-100 kyr ago (Fig. 2d) generally invigorated moisture flux onto the West African land mass, consistent with monsoon theory (*5*). Regional drying from ~100 kyr ago (*47*), culminating in severe drought ~80-70 kyr ago (*1,48*), may have resulted from the coincidence of still elevated temperature (Fig. 2d) with a by that time already weakened African monsoon, due to the slowdown of Atlantic meridional overturning circulation (AMOC; *49*) associated with incipient Northern Hemisphere glaciation (Fig. 2a).

Only one true MIS5 megadrought in eastern Africa

Our Lake Chala data show that the time window ~140-70 kyr ago in eastern tropical Africa was punctuated by three prolonged drought events, dated to 136.4±3.0 – 123.1±2.0 kyr ago, 110±2.0 –

97.5±0.5 kyr ago, and 85.4±1.5 – 76.6±1.4 kyr ago (Fig. 3d). Separated by ~23 kyr and each broadly synchronous with a precession-driven maximum in East Asian monsoon intensity (Fig. 3a), precipitation over eastern equatorial Africa during each of these episodes must have suffered from a precession-forced northward shift in mean annual position of the tropical rain belt (*3*), with high-amplitude precessional insolation forcing -due to high orbital eccentricity- producing large hydroclimate extremes (*1*,*10*). The first of these three major drought events is broadly coeval with the Last Interglacial period (MIS5e), except that drying set in ~136 kyr ago (Fig. 3d) shortly after local and southern-hemisphere warming associated with T2 (Fig. 2f,h), while the strength of the East Asian summer monsoon (Fig 3a) was impacted until ~130 kyr ago by continental cooling over Eurasia associated with Heinrich Stadial 11 (HS11; *50*).

Predominance of low BIT-index values (93% < 0.4; n = 277) and near-continuity of cm-scale banded sedimentation between ~136 and ~76 kyr ago (Fig. 3d and 3f) indicate that relatively dry climate conditions prevailed in eastern equatorial Africa throughout most of MIS5. Yet high-resolution seismic stratigraphy attests to only one major drawdown of Lake Chala (*11*), which lasted from 110±2.0 to 97.5±0.5 kyr ago followed by recovery to high-stand conditions by 88±1.7 kyr ago (Fig. 3). Also Lake Tanganyika experienced a single and rather short-lived (~9000 years) major drawdown, which within dating uncertainty started around the same time (*6*; Fig. 3). Pending comprehensive analysis of all pertinent African climate-proxy records, our combined data indicate that the severity of only this second MIS5 drought event was amplified by the coincidence of an interglacial temperature regime near the Equator and reduced moisture advection from the, by that time, already cool Arabian Sea so as to become the principal early late Pleistocene megadrought in eastern Africa.

The causal mechanism of MIS5 megadrought generation proposed here would seem to limit its environmental impact to the portion of the African continent receiving Indian Ocean moisture brought on-land by northeasterly monsoon winds. More broadly, our results indicate that megadrought episodes in the MIS5 time window (*3*) are most likely regionally defined, due to monsoon dynamics being governed partly by conditions in adjacent oceans and partly by the relative impact of thermodynamic effects on local effective moisture, rather than as a pan-continental response to orbital forcing. Resolving whether MIS5 megadrought events documented from other parts of tropical Africa involved a similar combination of climate-dynamical processes will require climate archives with a comparably strong chronological control, and paired reconstructions of temperature and hydroclimate to allow separating the processes driving variation in precipitation from those driving variation in continental evaporation.

Methods

The chronology of our high-resolution temperature and hydroclimate reconstructions is anchored in 170 radiometric age markers (^{14}C and ^{210}Pb) transferred from the 25-kyr climate-proxy record obtained by the Challacea project (*21*,*34*) to the DeepCHALLA drill site; local recovery of the 73.7-ka (*51*) Younger Toba Tuff (YTT) cryptotephra marker horizon (15); direct Ar/Ar dating of 10 visible tephra layers (*22*); and

local paleomagnetic signatures of six known magnetic field intensity excursions (*23*) which have been dated by ^{14}C or Ar/Ar methods elsewhere (*52-53*). The Bayesian age model integrating all 187 absolute time markers was calculated in Bacon (*54*) using parameters guided by lithostratigraphic constraints based on demonstrated continuity of sediment accumulation (*11*) and the uniform texture and water content of fine-grained organic muds throughout the DeepCHALLA sequence (*16,55*).

Start and end of the MIS5 low-stand in Lake Chala were dated by linear interpolation between the seismic-stratigraphic signatures of two mass-wasting events (MWEs) bracketing this low-stand (MWE9 and MWE10; *11*) that can be correlated to turbidite horizons in the DeepCHALLA sediment sequence with thicknesses of respectively 12.8 cm and 78.0 cm (*55*).

Mean summer Temperature (MST) was reconstructed based on the distribution of brGDGTs, bacterial membrane lipids of which the molecular structure varies with temperature to maintain optimal biophysical properties, using a calibration based on globally-distributed recent lake sediments (*14*), and rescaled to match LGM-to-Holocene temperature variation in eastern Africa as derived from GDGT-based temperature records at seven other lakes (*15*). Sampling procedure and analysis of sedimentary GDGTs has been described in detail elsewhere (*15*). Although the complete DeepCHALLA sequence covers the last ~250 kyr (*22*; Fig. S2), this study is limited to the last 170 kyr because different basin hydrology and water-column structure of Lake Chala before that time limited the climatic sensitivity of the aquatically-produced GDGTs (*16*). Additionally, 16 sampled and analysed sediment horizons were later determined to contain >25% of turbidite material (*56*), and were excluded from the proxy time series to ensure that all data represent sediments with primary deposition at the coring location (*15-16*). Therefore, the final 170-kyr DeepCHALLA climate-proxy time series comprise 776 data points. Due to stable linear sediment accumulation at multi-millennial time scale (Fig. S2), temporal resolution is fairly uniform at ~215 years.

Periodicity analysis of the 170-kyr Lake Chala MST and BIT-index reconstructions was performed on 35% detrended data series to minimize the influence of long-term trends, using REDFIT (*57*) with a rectangular type spectral window, an oversampling factor of 9 and a bandwidth of 6 dB. Variation in periodicities through time was revealed by a continuous wavelet transform using a Morlet function.

HadCM3 (Hadley Centre Coupled Model, version 3) climate-model simulations producing output presented here were performed by ref. *29* and considered the combined influence of insolation (*24*), atmospheric CO_2 concentration (*25*) and Northern Hemisphere ice volume (*58*) on sea-surface temperature during MIS5 with a time interval of 2 ka and spatial resolution of 1.25° ´ 1.25° Long/Lat; and on precipitation amount and seasonality in the 2.5° ´ 3.75° grid cell containing Lake Chala. The reference modern-day climate is based on the last 30 years of a Pre-Industrial (1850 CE) simulation run for 630 years, which compares well with NOAA-CIRES-DOE 20th-century climate reanalysis data (*59-60*).

Declarations

Acknowledgements

Recovery of the Lake Chala sediment record was facilitated by the government of Kenya through permit P/16/7890/10400 from the National Commission for Science, Technology and Innovation (NACOSTI), license EIA/PSL/3851 from the National Environmental Management Authority (NEMA), and research passes for foreign nationals issued by the Department of Immigration; and by the government of Tanzania through permits NA-2016-67 (270-285) and NA-2016-201 (277-292) from the Tanzania Commission for Science & Technology (COSTECH), permit EIA/10/0143/V.I/04 from the National Environmental Management Council, and resident permits issued by the Immigration Department. The authors wish to thank the Lands and Settlement Office of Taita-Taveta County (Kenya) to use government land as staging area; the institutions of our DeepCHALLA partners in Kenya and Tanzania for project facilitation; Caxton Mukhwana Oluseno, the 'Air Force One' team, the Kamba and Taveta communities of Lake Chala area, and DeepCHALLA field scientists for assistance in recovering the sediment record of Lake Chala; the National Lacustrine Core Facility (LacCore) at the University of Minnesota (USA) for organizing the logging and initial processing of core samples; and Anchelique Mets and Jessica Riekenberg (NIOZ) for analysis of sedimentary biomarkers.

Funding statement

This research was co-financed by NESSC Gravitation Grant 024.002.001 from the Dutch Ministry of Education, Culture and Science (OCW) to JSSD; by Ghent University Collaborative Research Operation grant BOF13/GOA/023, Hercules infrastructure grant AUGE/15/14-G0H2916N from the Research Foundation of Flanders, and a Francqui research professor mandate to DV; and by ICDP through the DeepCHALLA project (https://www.icdp-online.org/projects/world/africa/lake-challa/). QY and ZW acknowledge support from the Fonds de la Recherche Scientifique (FNRS, Belgium).

References

1. Scholz, C. A. et al. East African megadroughts between 135 and 75 thousand years ago and bearing on early-modern human origins. *Proc. Nat. Acad. Sci. USA* **104**, 16416–16421 (2007).
2. Cohen, A. S. et al. Ecological consequences of early Late Pleistocene megadroughts in tropical Africa. *Proc. Nat. Acad. Sci. USA* **104**, 16422–16427 (2007).
3. Blome, M. W., Cohen, A. S., Tryon, C. A., Brooks, A. S. & Russell, J.. The environmental context for the origins of modern human diversity: A synthesis of regional variability in African climate 150,000-30,000 years ago. *J. Hum. Evol.* **62**, 563–592 (2012).
4. Rito, T. et al. The first modern human dispersals across Africa. *PLoS ONE* **8**, e80031 (2013).
5. Kutzbach, J. E. Monsoon climate of the early Holocene: climate experiment with the earth's orbital parameters for 9000 years ago. *Science* **214**, 59-61 (1981).
6. McGlue, M. M. et al. Seismic records of late Pleistocene aridity in Lake Tanganyika, tropical East Africa. *J. Paleolimnol.* **40**, 635-653 (2008).
7. Moernaut, J. et al. The seismic-stratigraphic record of lake-level fluctuations in Lake Challa: Hydrological stability and change in equatorial East Africa over the last 140 kyr. *Earth Planet. Sci.*

Lett. **290**, 214-223 (2010).

8. Loomis, S. E. et al. The tropical lapse rate steepened during the Last Glacial Maximum. *Sci. Adv.* **3**, e1600815 (2017).
9. Gasse, F., Chalié, F., Vincens, A., Williams, M. A. J. & Williamson, D. Climatic patterns in equatorial and southern Africa from 30,000 to 10,000 years ago reconstructed from terrestrial and near-shore proxy data. *Quat. Sci. Rev*. **27**, 2316–2340 (2008).
10. Kutzbach, J. E. et al. African climate response to orbital and glacial forcing in 140,000-y simulation with implications for early modern human environments. *Proc. Nat. Acad. Sci. USA* **117,** 2255-2264 (2020).
11. Maitituerdi, A., Van Daele, M., Verschuren, D., De Batist, M. & Waldmann, N. Depositional history of Lake Chala (Mt. Kilimanjaro, equatorial East Africa) from high-resolution seismic stratigraphy. *J. Afr. Earth Sci.* **189**, 104499 (2022).
12. Wainwright, C. M. et al. 'Eastern African Paradox' rainfall decline due to shorter not less intense Long Rains. *NPJ Clim. Atmos. Sci.* **2**, 34 (2019).
13. Schouten, S., Hopmans, E. C. & Sinninghe Damsté, J. S. The organic geochemistry of glycerol dialkyl glycerol tetraether lipids: a review. *Org. Geochem*. **54**, 19–61 (2013).
14. Pearson, E. J. et al. A lacustrine GDGT-temperature calibration from the Scandinavian Arctic to Antarctic: Renewed potential for the application of GDGT-paleothermometry in lakes, *Geochim. Cosmochim. Acta* **75**, 6225–6238 (2011).
15. Baxter, A. J. et al. Reversed Holocene temperature–moisture relationship in the Horn of Africa. *Nature* **620**, 336–343 (2023).
16. Baxter, A. J., Verschuren, D., Peterse, F., Sinninghe Damsté J. S. Disentangling the influences of climate variability and lake-basin evolution on isoprenoid and branched GDGTs and their derived proxies: the 250-ka Lake Chala record. *Biogeosciences* **21**, 2877–2908 (2024).
17. Hopmans, E. C. et al. A novel proxy for terrestrial organic matter in sediments based on branched and isoprenoid tetraether lipids. *Earth Planet. Sci. Lett*. **224**, 107–116 (2004).
18. Rinke et al. A standardized archaeal taxonomy for the Genome Taxonomy Database. *Nat. Microbiol*. **6**, 946–959 (2021).
19. van Bree L. G. J. et al. Seasonal variability and sources of in situ brGDGT production in a permanently stratified African crater lake. *Biogeosciences* **17**, 5443–5463 (2020).
20. Baxter, A. J. et al. Seasonal and multi-annual variation in the abundance of isoprenoid GDGT membrane lipids and their producers in the water column of a meromictic equatorial crater lake (Lake Chala, East Africa). *Quat. Sci. Rev*. **273**, 107263 (2021).
21. Blaauw, M. et al. High-resolution ^{14}C dating of a 25,000-year lake-sediment record from equatorial East Africa. *Quat. Sci. Rev*. **30**, 3043–3059 (2011).
22. Martin-Jones, C. et al. The >250-kyr Lake Chala record: A tephrostratotype correlating archaeological, palaeoenvironmental and volcanic sequences across eastern Africa. *Quat. Sci. Rev*.

326, 108476 (2024).

23. Di Chiara, A. et al. A continuous 150-kyr record of geomagnetic field variations from Lake Chala, eastern equatorial Africa. *Geochem., Geophys., Geosyst*. **26**, e2024GC011933 (2025).
24. Berger, A. & Loutre, M.-F. Insolation values for the climate of the last 10 million years. *Quat. Sci. Rev*. **10**, 297–317 (1991).
25. Lüthi, D. et al. High-resolution carbon dioxide concentration record 650,000-800,000 years before present. *Nature* **453**, 379-382 (2008).
26. Barker, S. et al. 800,000 years of abrupt climate variability. *Science* **334** (2011).
27. EPICA Community Members. One-to-one coupling of glacial climate variability in Greenland and Antarctica. *Nature* **444**, 195-198 (2006).
28. Lisiecki, L. E. & Raymo, M. E. A Pliocene-Pleistocene stack of 57 globally distributed benthic $\delta^{18}O$ records. *Paleoceanography* **20**, PA1003 (2005).
29. Lyu A.Q. & Yin Q.Z. The spatial-temporal patterns of East Asian climate in response to insolation, CO_2 and ice sheets during MIS-5. *Quat. Sci. Rev*. **293**, 107689 (2022).
30. Oyabu, I. et al. The Dome Fuji ice core DF2021 chronology (0–207 kyr BP). *Quat. Sci. Rev*. **294**, 107754 (2022).
31. Hoffman, J. S., Clark, P. U., Parnell, A. C. & He, F. Regional and global sea surface temperatures during the last interglaciation. *Science* **355**, 276–279 (2017).
32. Thomas, Z. A. et al. Tipping elements and amplified polar warming during the Last Interglacial. *Quat. Sci. Rev*. **233**, 106222 (2020).
33. Berke, M. A. et al. Molecular records of climate variability and vegetation response since the Late Pleistocene in the Lake Victoria basin, East Africa. *Quat. Sci. Rev*. **55**, 59–74 (2012).
34. Lambert, F., Bigler, M., Steffensen, J. P., Hutterli, M. & Fischer, H. Centennial mineral dust variability in high-resolution ice core data from Dome C, Antarctica. *Clim. Past* **8**, 609–623 (2012).
35. Verschuren, D. et al. Half-precessional dynamics of monsoon rainfall near the East African Equator. *Nature* **462**, 637–641 (2009).
36. Chevalier, M. & Chase, B. M. Southeast African records reveal a coherent shift from high- to low-latitude forcing mechanisms along the east African margin across last glacial-interglacial transition. *Quat. Sci. Rev*. **125**, 117-130 (2015).
37. Buckles, L. K. et al. Interannual and (multi-) decadal variability in the sedimentary BIT index of Lake Challa, East Africa, over the past 2200 years: assessment of the precipitation proxy. *Clim. Past* **12**, 1243-1262 (2016).
38. Wang, P. X. et al. The global monsoon across time scales: mechanisms and outstanding issues. *Earth-Sci. Rev*. **174**, 84-121 (2017).
39. Brutsaert, W. Global land surface evaporation trend during the past half century: Corroboration by Clausius-Clapeyron scaling. *Adv. Water Resour*. **106**, 3-5 (2017).

40. Held, I. M. & Soden, B. J. Robust responses of the hydrological cycle to global warming. *J. Clim*. **19**, 5686–5699 (2006).
41. Nicholson, S. E. Climate and climatic variability of rainfall over eastern Africa. *Rev. Geophys*. **55**, 590–635 (2017).
42. Park, J. et al. Sub-annual resolution evidence for limited impact of the 74-ka Toba eruption on eastern African climate. *Sci. Adv*. (pending acceptance after 3rd review).
43. Schaebitz, F. et al. Hydroclimate changes in eastern Africa over the past 200,000 years may have influenced early human dispersal. *Comm. Earth Envir*. **2**, 1–10 (2021).
44. Roberts, H. M. et al. Using multiple chronometers to establish a long, directly-dated lacustrine record: constraining >600,000 years of environmental change at Chew Bahir, Ethiopia. *Quat. Sci. Rev.* **266**, 107025 (2021).
45. Tierney, J. E., deMenocal, P. B. & Zander, P. D. A climatic context for the out-of-Africa migration. *Geology* **45**, 1023-1026 (2017).
46. Weldeab, S., Lea, D. W., Schneider, R. R. & Andersen, N. 155,000 years of West African monsoon and ocean thermal evolution. *Science* **316**, 1303-1307 (2007).
47. Miller, C. S., Gosling, W. D., Kemp, D. B., Coe, A. L. & Gilmour, I. Drivers of ecosystem and climate change in tropical West Africa over the past ~540 000 years. *J. Quat. Sci*. **31**, 671-677 (2016).
48. Shanahan, T. M. et al. Age models for long lacustrine sediment records using multiple dating approaches – an example from Lake Bosumtwi, Ghana. *Quat. Geochronol*. **15**, 47-60 (2013).
49. Chang, P. et al. Oceanic link between abrupt changes in the north Atlantic Ocean and the African monsoon. *Nat. Geosci*. 1, 444-448 (2008).
50. Cheng, H. et al. The Asian monsoon over the past 640,000 years and ice age terminations. *Nature* **534**,640-646 (2016).
51. Mark, D. F. et al. High-precision $^{40}Ar/^{39}Ar$ dating of pleistocene tuffs and temporal anchoring of the Matuyama-Brunhes boundary. *Quat. Geochronol*. **39**, 1-23 (2017).
52. Singer, B. S. A Quaternary geomagnetic instability time scale. *Quat. Geochronol*. **21**, 29-52 (2014).
53. Channell, J. E. T., Singer, B. S. & Jicha, B. R. Timing of Quaternary geomagnetic reversals and excursions in volcanic and sedimentary archives. *Quat. Sci. Rev*. **228**, 106114 (2020).
54. Blaauw, M. & Christen, J. A. Flexible paleoclimate age-depth models using an autoregressive gamma process. *Bayesian Anal*. **6**, 457–474 (2011).
55. Maitituerdi, A. *Depositional history of Lake Chala (Mt. Kilimanjaro, equatorial east Africa): reference frame for a high-resolution, ~250 kyr paleoenvironmental archive*. Unpubl. PhD thesis, University of Haifa, Israel (2023).
56. Swai, V. Lake Chala statigraphy: Developing a method to identify and quantify surficial slope sediment remobilization. Unpubl. MSc thesis, Ghent University, Belgium (2018).
57. Schulz, M. & Mudelsee, M. REDFIT: Estimating red-noise spectra directly from unevenly spaced paleoclimatic time series. *Comput. Geosci*. **28**, 421-426 (2002).

58. Ganopolski, A. & Calov, R. The role of orbital forcing, carbon dioxide and regolith in 100-kyr glacial cycles. *Clim. Past* **7**, 1415-1425 (2011).
59. Compo, G.P. et al. The twentieth century reanalysis project. *Q. J. R. Meteorol. Soc*. **137**, 1-28 (2011).
60. Slivinski, L.C. et al. Towards a more reliable historical reanalysis: improvements for version 3 of the twentieth century reanalysis system. *Q. J. R. Meteorol. Soc.* **145**, 2876-2908 (2019).
61. National Oceanic and Atmospheric Administration. Long-term Mean Sea Surface Data, https://psl.noaa.gov/data/gridded/data.noaa.oisst.v2.highres.html.
62. Bereiter, B. et al. Revision of the EPICA Dome C CO_2 record from 800 to 600-kyr before present. *Geophys. Res. Lett*. **42**, 542-549 (2015).

Figures

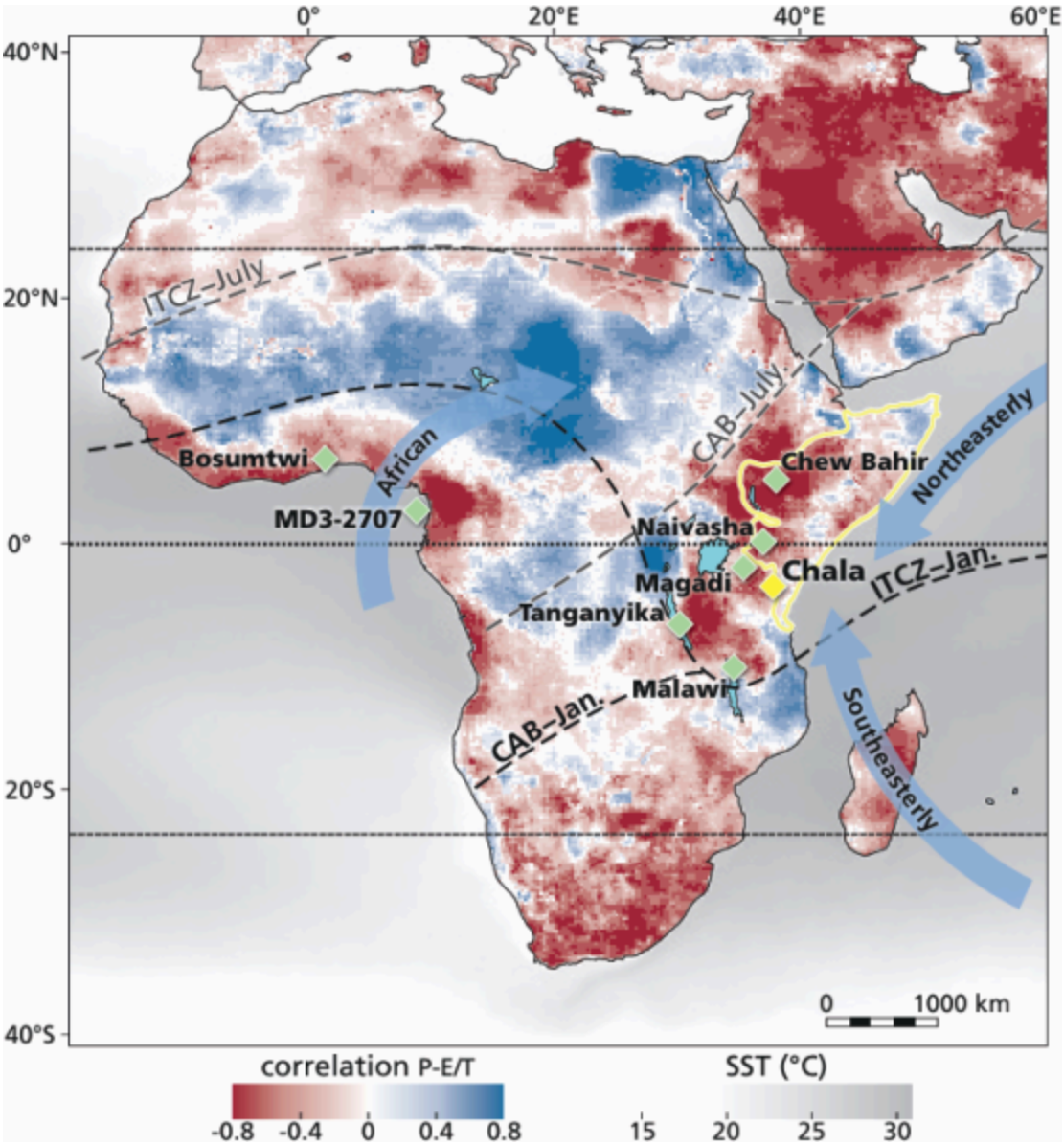


Figure 1

Location of Lake Chala (yellow diamond) and selected other paleoclimate archives (green diamonds) in relation to synoptic climatology over the African continent and adjacent oceans. Blue and red hues on the continents display the correlation between annual effective moisture (P − E) and annual temperature (T) in observational data over the period 1980–2021, downscaled to 0.25° resolution (*15*). Values exceeding 0.4 are significant at $P < 0.01$. Grey hues over the oceans reflect annual-mean SSTs, with values exceeding 23 °C delineating the tropics (*61*). Dashed lines show the approximate positions of the Intertropical Convergence Zone (ITCZ) and Congo Air Boundary (CAB) in January (black) and July (grey), and blue arrows the dominant seasonal wind directions associated with the three main monsoon systems (Fig. S1). Yellow contour delineates the Horn of Africa region of eastern Africa which fully depends on Indian Ocean moisture (*12*).

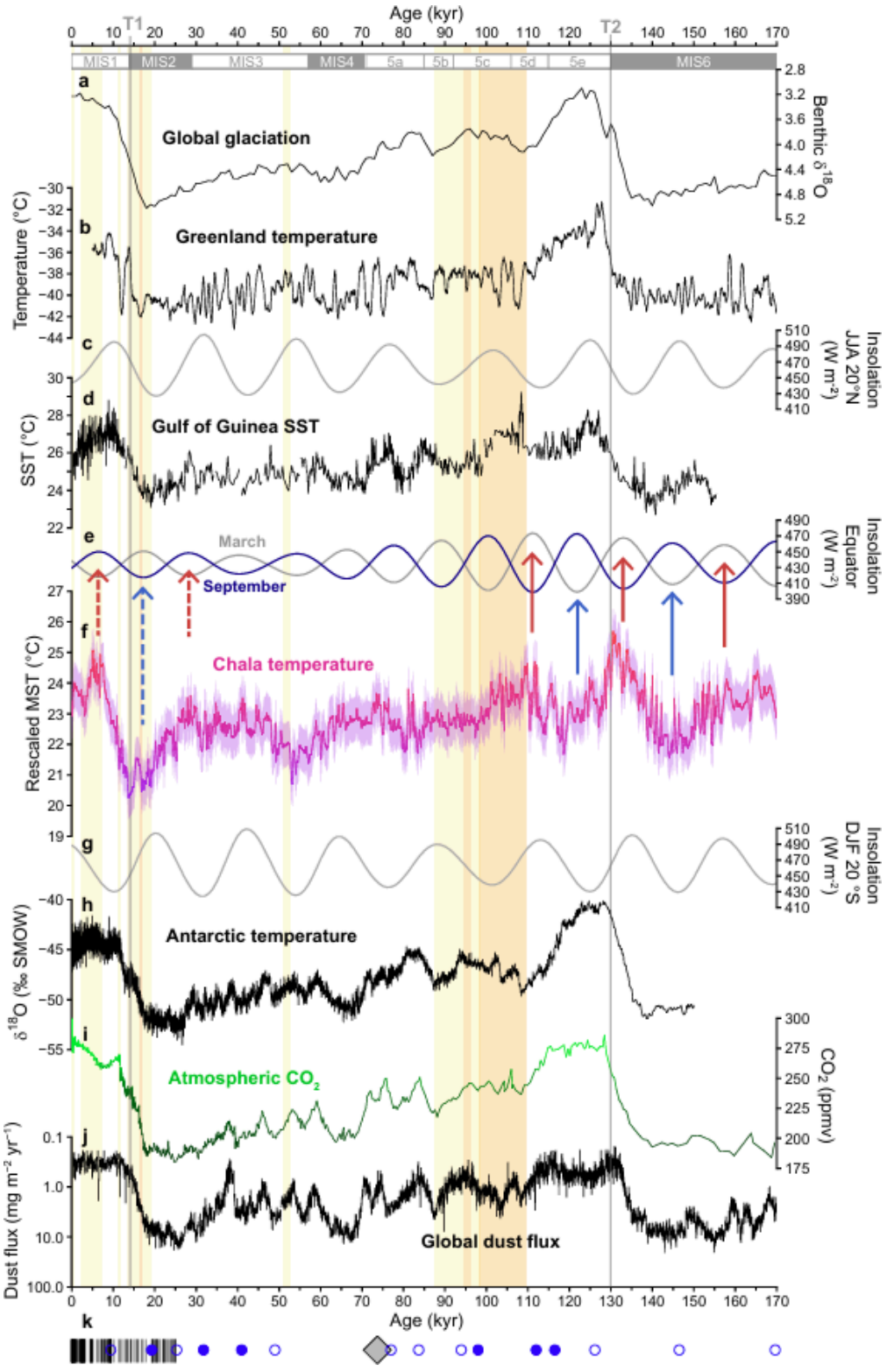


Figure 2

170,000-year temperature reconstruction for eastern equatorial Africa in relation to orbital insolation and palaeoclimate reference records. **a**, Benthic marine d^{18}O stack (*28*) reflecting variation in global ice volume (i.e., glaciation) and defining the timing of marine isotope stages (MIS6-MIS1), substages (MIS5e-MIS5a) and glacial terminations (T2, T1; grey vertical lines). **b**, Synthetic Greenland ice-core d^{18}O record reflecting Arctic temperature history (*26*). **c**, Mean daily insolation for the months of July, July and

August at 20°N, reflecting variation in boreal summer insolation (*24*). **d**, Sea surface temperature (SST) reconstruction for the eastern equatorial Atlantic Ocean, based on Mg/Ca ratios in core MD03-2707 from the Gulf of Guinea (*46*). **e**, Mean daily insolation for the months of March (grey) and September (blue) at the equator (*24*). **f**, Temperature (MST) reconstruction for eastern equatorial Africa based on sedimentary brGDGTs from Lake Chala, rescaled using an eastern African ensemble reconstruction for the last 25 kyr (*15*). Purple-to-red shading represents the ±0.7 °C root mean square error (RMSE) uncertainty envelope of the temperature calibration (*14*) after rescaling, with grading purple-red transition at 23 °C. Bold arrows show the probable (full) and apparent (dashed) association between equatorial temperature minima (blue) and maxima (red) and local March or September minima/maxima. **g**, Mean daily insolation for the months of December, January and February at 20°S, reflecting variation in austral summer insolation (*24*). **h**, Ice-core $d^{18}O$ record from Dronning Maud Land (*27*), reflecting temperature variation in Antarctica. **i**, Atmospheric CO_2 concentration recorded in Antarctic ice (*25*) on time scale AICC2012 (*62*), with shift from dark to light green centered on 255 ppm. **j**, Global dust flux recorded in Antarctic ice (*34*). **k**, Age anchors based on radiocarbon dating (thin vertical lines), Ar/Ar dating (filled circles), locally registered paleomagnetic intensity excursions (empty circles) and local cryptotephra of the 73.7-kyr Toba eruption (grey diamond) supporting age-model construction (Fig. S1; Methods).

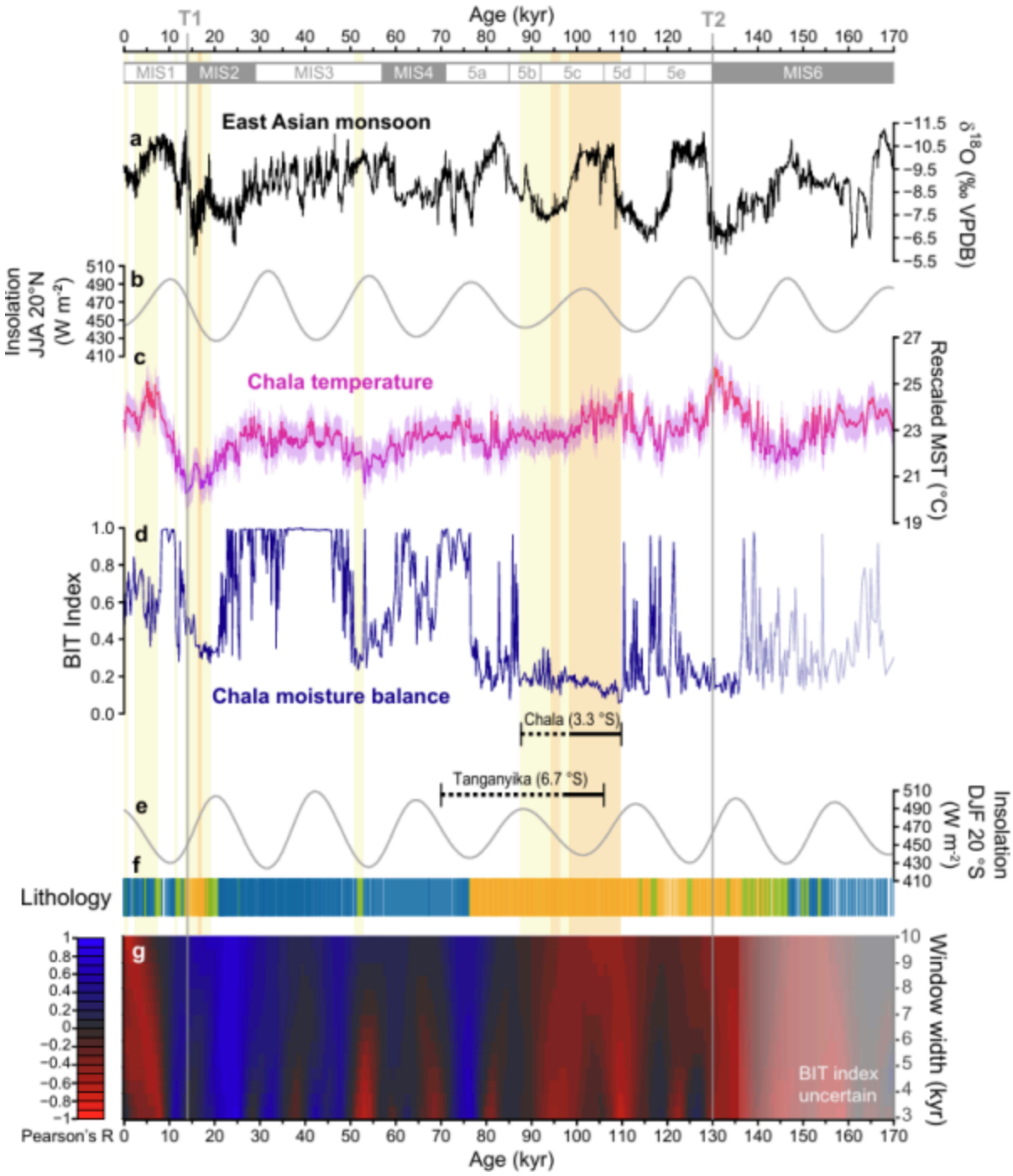


Figure 3

170,000-year moisture-balance reconstruction for eastern equatorial Africa in relation to orbital insolation and palaeoclimate reference records. **a**, Speleothem composite d^{18}O record reflecting East Asian summer monsoon intensity (*50*). **b**, Mean daily insolation for the months of July, July and August at 20°N, reflecting variation in boreal summer insolation (*24*). **c**, Temperature (MST) reconstruction for eastern equatorial Africa based on sedimentary brGDGTs from Lake Chala, as in Fig. 2f. **d**, Moisture-balance reconstruction for eastern equatorial Africa based on BIT-index variation in sedimentary GDGTs from Lake Chala; BIT-index variation prior to ~140 kyr ago (stippled line) is considered less robust as moisture-balance proxy (Supplementary Information). **e**, Mean daily insolation for the months of

December, January and February at 20°S, reflecting variation in austral summer insolation (*24*). **f**, Lithology of the sediment sequence showing the distribution of mm-scale laminated (blue) and cm-scale banded (dark yellow) facies, and sections with frequent alternation between them (green). **g**, Evolving Pearson correlation (*36*) between reconstructed moisture balance (BIT) and temperature (MST) in eastern equatorial Africa, using sliding bin widths varying between 3 and 10 kyr. Vertical shaded bars show the timing of moderate (yellow) to pronounced (orange) low-stands of Lake Chala evidenced by seismic stratigraphy (7,11; Fig. S2). Also indicated is the timing of pronounced early Late Pleistocene low-stand (solid line) and recovery (dotted line) in Lake Tanganyika (*1,6*) for comparison with our data.

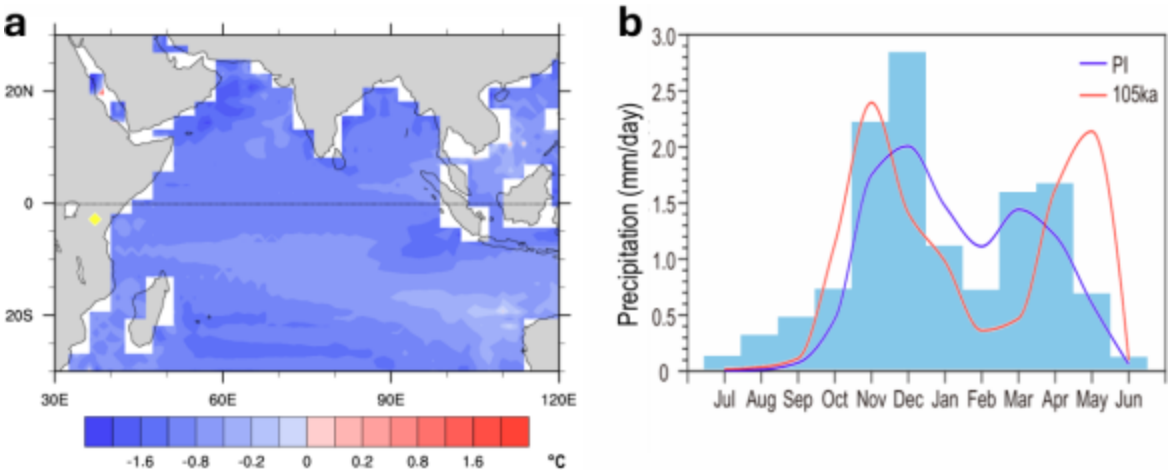


Figure 4

Sea-surface temperature anomaly and rainfall seasonality during early Late Pleistocene African megadrought. a, HadCM3-simulated (*29*) annual-mean sea-surface temperature (SST) anomaly 105 kyr ago, showing greater cooling in the Arabian Sea compared to (Pre-Industrial) modern-day SSTs than in the equatorial western Indian Ocean, and hence steeper meridional SST gradient than today. **b**, Comparison between HadCM3-simulated (*29*) monthly precipitation (mm/day) in the 2.5° ´ 3.75° Lat/Long grid cell containing Lake Chala 105 kyr ago (red line) and today (Pre-Industrial, blue line), and correspondence of the latter with observed mean monthly precipitation today (mm/day, 1957-2007) as recorded at Voi, 80 km east of Lake Chala (light blue bars; *35*).

Supplementary Files

This is a list of supplementary files associated with this preprint. Click to download.

- ExtendedData.docx